PNAS RESEARCH ARTICLE | EARTH, ATMOSPHERIC, AND PLANETARY SCIENCES OPEN ACCESS

Human and climate impacts on the alpine Critical Zone over the past 10,000 y

William Rapuc[a,b,c,1], Damien Guinoiseau[c,d], Fabien Arnaud[a], Mathieu Dellinger[a,b], Pierre Sabatier[a], Jérôme Gaillardet[c], Jérôme Poulenard[a], and Julien Bouchez[c]

Affiliations are included on p. 7.

Edited by William Schlesinger, Cary Institute of Ecosystem Studies, Millbrook, NY; received March 17, 2025; accepted June 10, 2025

Agropastoral activities have impacted the habitable part of our planet—the "Critical Zone"—for thousands of years, triggering a major increase in soil erosion in mountain environments. Understanding and quantifying the impact of these activities on soil is central to the well-being of our societies. Here, we investigate the isotope ratios of the trace element lithium in detrital sediments of Lake Bourget, European Alps, and provide a reconstruction of the impact of human activities on the evolution of alpine soil during the Holocene. We demonstrate that during the Early Holocene, soil formation was altered by the development of pastoralism followed by tillage. This led to three major erosive surges (3.8 to 3.0, 2.8 to 1.6, and 1.6 ky cal BP to modern times), thinning soils down to a state close to that of their early development 10,000 y ago. The detailed study of the lithium detrital signal reveals the appearance of an altitudinal decoupling in the response of the Critical Zone in the Alps following the development of the agropastoral activities during the Iron Age. The onset of agropastoral activities disrupted the balance between soil formation and erosion, leading to erosion rates 3 to 10 times faster than soil production since the end of the Ice Age.

human impact | Anthropocene | soil evolution | erosion | lake sediments

Significance

Here, we use lithium isotopes preserved in lake sediments to reconstruct 9,500 y of soil development in the European Alps. By disentangling the respective roles of climate and agropastoral land use across a mountain catchment, we show that human activity began to dominate soil evolution around 3,800 y ago. This marks the onset of a pedological Anthropocene, where human activities accelerated soil degradation by up to an order of magnitude compared to natural soil formation rates. Our findings highlight how long-term lake sediment records can reveal the cumulative impacts of agriculture on the Critical Zone, insights that are likely relevant to other mountain regions worldwide and vital for guiding sustainable land-use strategies.

The Critical Zone, the layer of our planet sitting between the "rocks and the sky" (1), supports all terrestrial life and stores carbon during the development of soil through biogeochemical weathering (the rock-to-soil transformation process) and attendant organic matter sequestration (2, 3). Yet, since the onset of the Anthropocene and the intensification of land use for agriculture, the Critical Zone—and soils in particular—have been under major threat (4, 5). Understanding the effect of human activities on soil formation is essential for implementation of appropriate management policies (2, 3, 6). Among all the factors impacting soil over time, bioclimatic fluctuations and land use appear to be the most dominant on a decadal to thousands-year timescale (5, 7). However, whether specific human activities have become the primary driver of soil evolution, and if so, since when remains an open question.

Lake sediments offer a unique archive to reconstruct the trajectory of soils at relevant temporal (multi-100-y) and spatial (catchment) scales (8–10). Such evolution can be revealed by the combination of geochemical analysis and precise dating of the sediments (11, 12). This retrospective approach makes it possible to directly compare soil trajectories before the beginning of human influence as well as during periods of significant human forcings (12, 13). A major difficulty in quantifying the effect of human activities on soil trajectories lies in disentangling their impact from that of climate, given that both have evolved concomitantly since the onset of the Holocene (14). However, recent methodological developments, coupled with a strategic selection of study sites, allow for a more robust separation of anthropogenic and bioclimatic influences on soil erosion (12).

A further characterization of the effects of climate and human activity on soil requires probing of the relative rates of biogeochemical weathering and physical erosion. These processes determine whether soils are predominantly forming or degrading over time. The lithium isotopic composition (δ^7Li) of detrital sediments has emerged as a sensitive proxy for quantifying silicate weathering intensity and pedogenesis (15–17). The two lithium isotopes ^{6}Li and ^{7}Li are fractionated during biogeochemical weathering (18): ^{6}Li is preferentially incorporated into secondary minerals such as clays, whereas ^{7}Li becomes enriched in soil solutions and rivers (19). As a result, secondary weathering products (clays, oxides) typically exhibit lower δ^7Li values compared to their unweathered parent rock. Although relatively few studies report δ^7Li values in soils (20–25), current evidence suggests that increasing degrees of pedogenesis, characterized by enhanced formation of clay minerals, are associated with decreasing δ^7Li values in bulk soils (26).

Author contributions: W.R., F.A., P.S., J.G., and J.B. designed research; W.R., D.G., and M.D. performed research; W.R. and J.B. analyzed data; and W.R., D.G., F.A., M.D., P.S., J.G., J.P., and J.B. wrote the paper.

The authors declare no competing interest.

This article is a PNAS Direct Submission.

[1]To whom correspondence may be addressed. Email: william.rapuc@hotmail.fr.

This article contains supporting information online at https://www.pnas.org/lookup/suppl/doi:10.1073/pnas.2506030122/-/DCSupplemental.

Published July 14, 2025.

Here, we develop a multiproxy approach, combining lithium isotopes with major and trace element analyses, and a source-to-sink investigation of Lake Bourget to reconstruct soil evolution in the European Alps. This region provides an ideal natural laboratory (Fig. 1), as both human land-use history and regional bioclimatic variability since the Last Glacial Maximum are well documented (27, 28), thus constituting one of the rare global contexts where the respective impacts of anthropogenic activity and climate on soil erosion can be disentangled (12). We first characterize the lithium isotopic composition of the main sediment sources through analyses of representative bedrock and river sediments. We then correct for source-related δ^7Li variability in lake sediments in order to isolate the effects of physical erosion and biogeochemical weathering. On this basis, we reconstruct the relative influence of bioclimatic fluctuations and land use on soil development over the Holocene. Our findings demonstrate that, beyond merely accelerating soil erosion, humans have fundamentally altered through agropastoral activities both the nature and pace of soil-forming processes in the European Alps.

Study Site

Lake Bourget (Fig. 1) is fed by one of the largest catchments in the European Alps (4,976 km^2), extending from the lowlands of the Chambéry valley (230 m) to the high elevations of the Mont-Blanc massif (4,808 m), typifying alpine environments and their evolution through time (13). With a surface area of 44.5 km^2, it is one of the largest natural lakes in France. The lake receives inflow from three main rivers—the Leysse, Sierroz, and Tillet—and drains via a single outlet, the Canal de Savière, which connects it to the Rhône River. During flood events, the Rhône can backflow into the lake, and is the main contributor of detrital sediments to the lake (29).

The catchment can be broadly divided into two distinct lithological and geomorphological source areas: i) the glaciated, high-elevation Mont-Blanc massif, predominantly underlain by granitic bedrock (158 km^2, elevations between 2,300 and 4,808 m); and ii) the nonglaciated part of the catchment (3,804 km^2, <3,300 m), underlain by sedimentary rocks: schists, helminthoid flysch, marl, limestone, and sandstone, mainly of late Paleozoic and Mesozoic age. Limestone outcrop areas (1,014 km^2) do not supply significant detrital material to the lake and are excluded from sediment contribution estimates. The nonglaciated region has supported agropastoral land use for at least the past 7,000 y. These two regions are readily distinguishable through Nd isotopic source tracing (12, 30) (Fig. 1). Erosion dynamics in the glaciated region are assumed to depend exclusively on bioclimatic forcing, whereas those in the nonglaciated area reflect the combined influences of climate and human activity (12).

Among the various sedimentary sequences collected from Lake Bourget, we selected the LDB18&19 core, which provides a continuous record spanning the past 9,500 y. This sediment sequence was retrieved from the lake's depocenter and provides a spatially integrative archive of the catchment dynamics, owing to its low sedimentation rate and central location. Using a mixing model based on the neodymium isotope ratio (^{143}Nd/^{144}Nd), erosion rates were reconstructed for both the glaciated and nonglaciated regions of the catchment over time (12). This approach enabled a robust quantification of human-induced erosion rates within a highly erosive mountainous area (31).

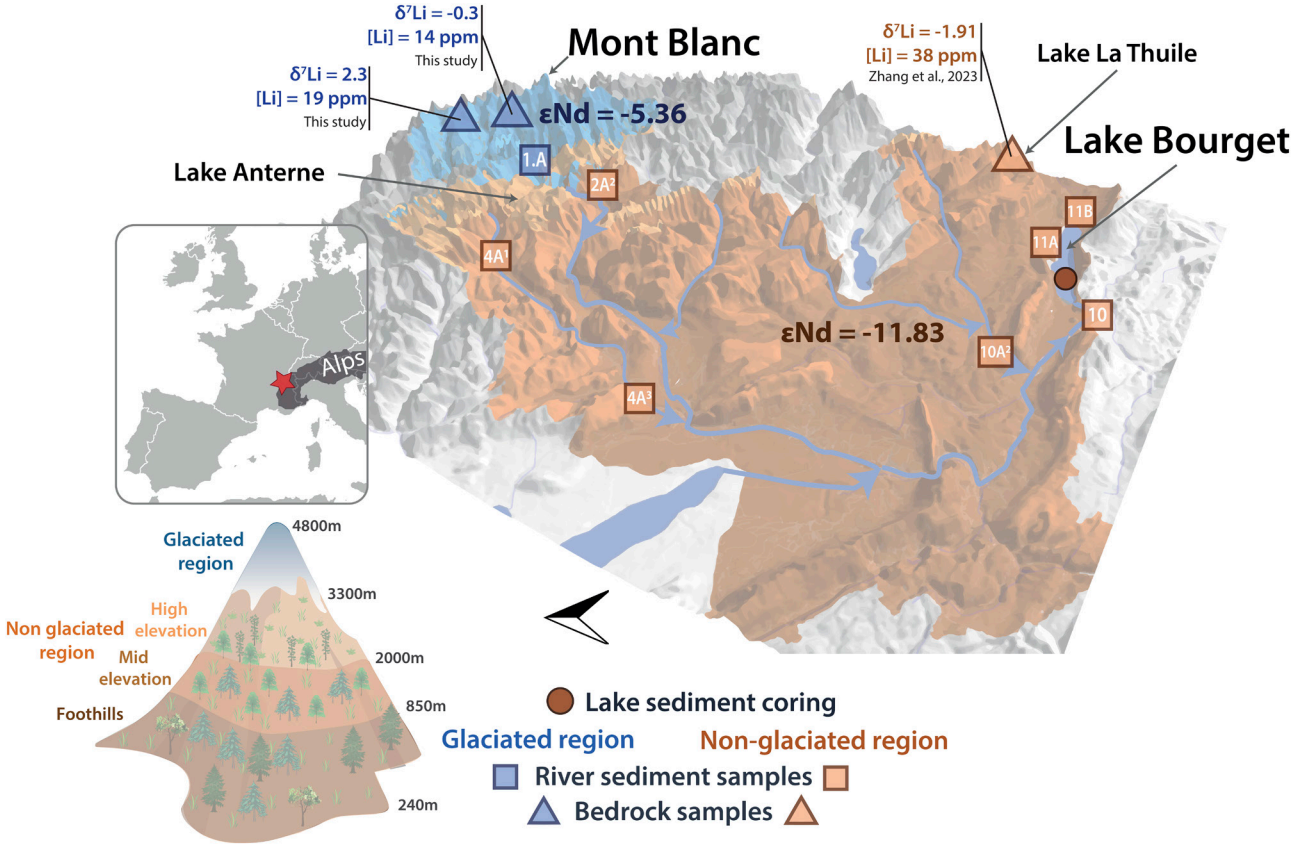

Fig. 1. 3D-view of Lake Bourget catchment with two distinct regions, each characterized by a specific lithology and geochemical signature. In the Lake Bourget catchment, erosion of the glaciated region is driven by bioclimate fluctuations, whereas the erosion in the nonglaciated region is impacted by both climate and human activities such as pastoralism and tillage. The data for the nonglaciated bedrock samples are obtained from a soil profile in the Lake La Thuile catchment (16), these data are in agreement with those obtained on river sediments in the area (this study). Neodymium isotope ratios (expressed as εNd values) are from measurements of river sediments in the catchment (12).

Results

The signature of sediment derived from the glaciated part of Lake Bourget catchment was obtained through the analysis of two granite samples from the glaciated Mont-Blanc Massif (32) yielding δ^7Li, [Li] and Li/Al values of −0.3 and +2.3 ‰, 14 and 19 ppm and 0.18 and 0.27 × 10^{-3} g/g, respectively (*Materials and Methods*). For the nonglaciated part of the catchment, we use data from Lake La Thuile, a small lake located at mid- elevations (874 m) within the Lake Bourget catchment and mostly underlained by marls, with reported values of δ^7Li = −1.9 ‰, [Li] = 38 ppm and Li/Al = 1.15 × 10^3 g/g for the marls (16) (Fig. 1 and *SI Appendix*, Table S3). The river sediment δ^7Li and Li concentration of Lake Bourget main tributaries, which capture lithological variability across subcatchments, range from +0.9 ‰ (δ^7Li) and 31 ppm ([Li]) for the river sample closest to the glaciated region to −2.0 ‰ (δ^7Li) and 37 ppm ([Li]) for the sample (Rhône River) closest to the inlet of Lake Bourget. The mean value for the rivers draining only the nonglaciated part of the catchment is δ^7Li = −0.9 ± 0.4 ‰ and [Li] = 36 ± 14 ppm (1 SD, n = 7). The river sediment samples from the nonglaciated regions display a mean Li/Al value of 0.87 ± 17 × 10^{-3} g/g, as opposed to a value of 0.52 × 10^{-3} g/g for the samples from rivers draining only the glaciated region (Fig. 2 and *SI Appendix*, Table S2).

Lacustrine sediments from Lake Bourget exhibit Li concentrations around 95 ± 48 ppm (1 SD, n = 27) and Li/Al values in the range 0.75 to 1.25 × 10^{-3} g/g (Fig. 2), in line with previously reported values for sediments derived from the erosion of sedimentary rock (33). The Li isotopic composition of these samples ranges from −3.8 ‰ to −2.1‰, with a median of −2.9 ± 0.4‰ (1 SD, n = 27). Throughout the Holocene, the δ^7Li_{LK} signal (LK: lake sediments) displays a decreasing trend from ca. 9.4 (−2.1 ‰) to ca. 5.6 kyrcal BP (−3.2 ‰). The δ^7Li_{LK} then gradually increases until 4.4 ky cal BP (−2.8 ‰) before stagnating until 3.8 ky cal BP (−3.0 ‰). Subsequently, the signal alternates between low values (3.6, 2.2, and 1.4 ky cal BP), followed by gradual increases in the signal leading to peaks (3, 1.8, and 0.2 ky cal BP), followed by further decreases (Fig. 3 and *SI Appendix*, Table S1).

Discussion

Assessing Grain Size and Source Rock Effects On The Lake Bourget δ^7Li Record. Reconstructing weathering over time with Li isotopes requires first to correct for any potential grain-size sorting during transport and deposition (33, 34). A previous study of Lake Bourget sediments found no significant variation in the grain size of detrital particles over the Holocene (35). Additionally, the fine fraction of Lake Bourget sediment δ^7Li is similar to that of the bulk fraction (*SI Appendix*, Fig. S1), making our sedimentary δ^7Li record internally consistent with respect to sorting.

Whereas the preferential transport of fine particles during periods of low erosion clearly influences the δ^7Li signal in the small (1.6 km^2) alpine catchment of Lake La Thuile (18) leading to a decrease of one per mil within a millennia at that site, the lack of correlation between selective transport proxies and δ^7Li_{LK} in Lake Bourget suggests no significant effect of selective transport here (r^2 = 0.007, *P*-value = 10^{-31} for Al/Ti and r^2 = 0.028, *P*-value = 10^{-13} for Al/Zr; *SI Appendix*, Fig. S2). We propose that this difference is related to the much larger catchment size for Lake Bourget, with selective transport unlikely to be a concern over such a large area where erosion has remained high throughout the Holocene.

Next, we investigate whether a change of the dominant bedrock source can influence the δ^7Li_{LK} signal in Lake Bourget. To address this, we correct the δ^7Li_{LK} signal for the varying contribution of the glaciated region (f_G) to obtain the δ^7Li of the nonglaciated region (δ^7Li_{NG}). In doing so, we assume that the Li concentration

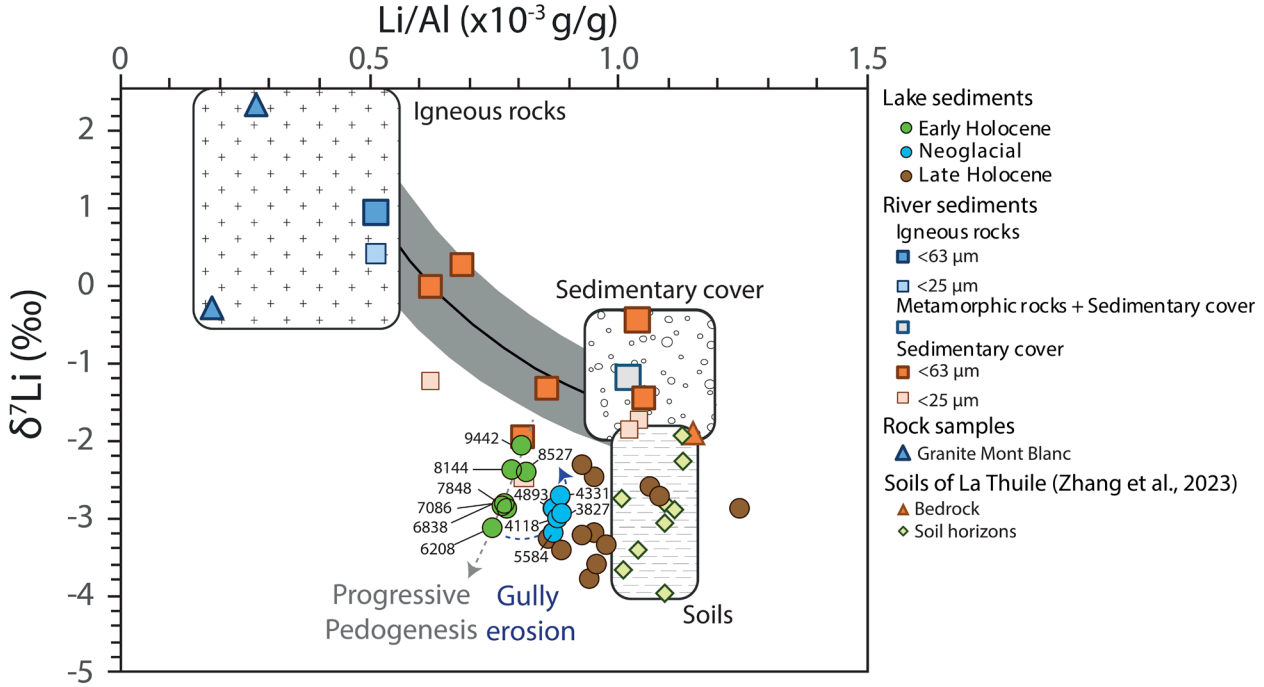

Fig. 2. δ^7Li vs. Li/Al ratio of river and lake sediment samples from the Lake Bourget catchment. A mixing model allows us to describe the trend between granite from the glaciated region of the catchment, and the sedimentary cover from the nonglaciated part of the catchment (gray area). The soil and bedrock values are from the Lake La Thuile catchment (Fig. 1) (16). Lake sediment samples are divided into three different periods: Early Holocene (9,442 to 6,208 y cal BP), Neoglacial (5,584 to 3,827 y cal BP), and the Late Holocene (3,548 y cal BP to present days).

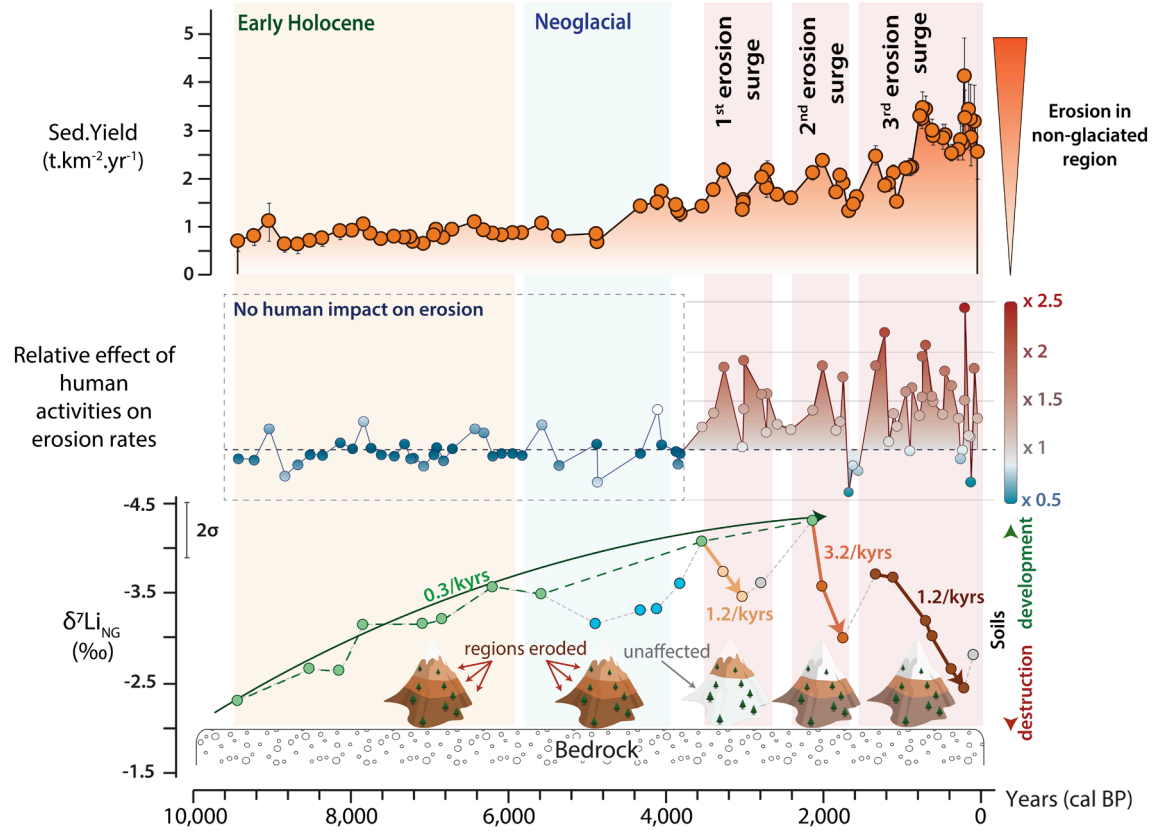

Fig. 3. Erosion and weathering in the Lake Bourget catchment throughout the Holocene. Erosion signal in $t.km^{-2}.y^{-1}$ compared with the relative effect of human activities on erosion rates obtained from a previous study (12) and the δ^7Li signal of lake sediments. The δ^7Li signal is interpreted as recording an initial phase of soil development between 9.5 and 3.8 ka cal BP, interrupted only by a shift to colder and wetter conditions during the Neoglacial period (5.8 to 3.8 ka cal BP), when gully-type erosion dominate. Three subsequent surges of intense erosion, attributed to human activity, are identified after 3.8 ka cal BP. These events affected areas at different elevations within the catchment and progressively returned soils to a state comparable to that observed immediately after deglaciation. The δ^7Li record reveals a marked imbalance between soil formation and destruction rates, with human-driven processes destructing soils 3 to 10 times faster than their natural rate of formation.

in the nonglaciated area ($[Li]_{NG}$) remained constant over the study time period. Building on previous work (12), we use a binary mixing model derived from an Nd isotope mass balance (12) yielding the sediment contributions from both the glaciated and nonglaciated regions (f_{NG}):

$$f_G + f_{NG} = 1, \quad [1]$$

$$[Li]_{LK} = [Li]_G \times f_G + [Li]_{NG} \times f_{NG}, \quad [2]$$

$$\delta^7Li_{NG} = \frac{\delta^7Li_{LK} \times [Li]_{LK}}{[Li]_{NG} \times f_{NG}} - \frac{\delta^7Li_G \times [Li]_G \times f_G}{[Li]_{NG} \times f_{NG}}. \quad [3]$$

We hypothesize that the δ^7Li signature and the Li concentration of sediments derived from the glaciated area of the Lake Bourget catchment have remained stable over the Holocene, as no soil has developed at these high-elevation, ice-covered locations (36). This assumption is supported by the similarity in δ^7Li values between the granites of the Mont-Blanc massif (+1.0 ‰) and the modern Arve River sediment collected at the foot of the massif (+0.9 ‰). As this sediment reflects a mixture of rocks from the massif, we consider its δ^7Li value representative of the glaciated region's source rock. For the nonglaciated region, we used the [Li] value from a marl sample within the Lake Bourget catchment (16), that is equivalent to the mean [Li] of the river sediments in the nonglaciated region (38 and 36 ppm, respectively). We find that the effect of variable contribution from the glaciated region on δ^7Li_{LK} signal appears to be negligible (*SI Appendix*, Fig. S3) as the uncorrected and the corrected signals are highly correlated (r^2 = 0.97, *P*-value = 10^{-13}) and the difference between the two curves is less than the typical analytical uncertainty on the δ^7Li_{LK} record (*SI Appendix*, Fig. S3).

Climate Effect on Soil Development in the Western European Alps. We characterize soil evolution at the catchment scale using the δ^7Li vs. Li/Al ratio framework (33, 34, 37). As shown in Fig. 2, sediments from Lake Bourget plot below the mixing line defined by the catchment's two primary lithological sources. Between 9.5 and 6.2 ky cal BP, a clear decreasing trend in both δ^7Li and Li/Al is observable in lake sediments (from −2.3 to −3.6 ‰ and from 0.81 to 0.75 × 10^{-3} g/g, respectively), progressively diverging from the source mixing array. Such a trend has previously been interpreted as reflecting an increase in weathering intensity—that is, a higher ratio of chemical to physical erosion (33, 34, 37). When compared with modern calibrations from large river systems (34), the ~1‰ decrease in δ^7Li corresponds to an approximately threefold increase in weathering intensity (*SI Appendix*, Fig. S4). This δ^7Li decrease mirrors the trend recorded in sediments from Lake La Thuile draining a small, mid-elevation catchment within the Lake Bourget catchment (16) (Fig. 1 and *SI Appendix*, Fig. S5). An increase in weathering intensity under low-erosion conditions can result from either i) enhanced formation of secondary minerals, typically associated with deepening of the weathering profile and soil thickening, or ii) increased mineral dissolution in already-developed soils, without further soil development. Given the asynchronous deglaciation across elevations since the Last Glacial Maximum (38),

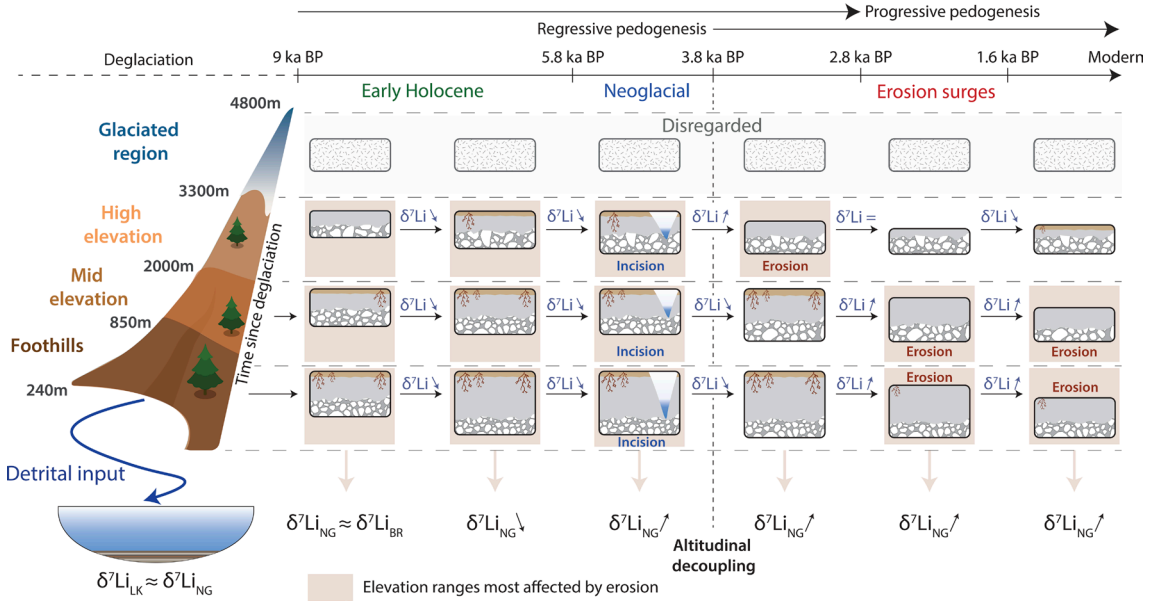

Fig. 4. Diagram of soil evolution in the Lake Bourget catchment for the last 9.5 ky. Soil development in the catchment followed deglaciation, with a progressive pedogenic evolution modulated by elevation. This pattern, consistent with observations elsewhere in the Alps, reflects a chronosequence from Lithosols and Regosols to Cambisols, and eventually Podzols. As a result, soils at different stages of development coexist along the altitudinal gradient. Pedogenesis continued until the Neoglacial period (5.8 to 3.8 ky cal BP), when a shift to a wetter climate induced incision confined to riverbeds, without significantly altering lateral soil development. From approximately 3.8 ky cal BP onward, however, human activities became a major geomorphic force, initiating three distinct erosive surges. These began with the degradation of surface soil horizons, followed by the remobilization of deeper material. The first surge (3.8 to 2.8 ky cal BP), linked to the onset of pastoralism, primarily affected high-elevation zones. The subsequent surges (2.8 to 1.6 ky cal BP) were associated with the expansion of agriculture and impacted mid- and low-elevation soils. This scenario was produced by combining the interpretations derived from the δ^7Li_{NG} signal and the information available on the intensity of agropastoral activities by altitudinal level (*SI Appendix*, Fig. S6). δ^7Li_{BR} corresponds to the isotopic signature of the bedrock.

it is likely that both mechanisms operated concurrently across the catchment, contributing to what can be described as progressive soil development (8).

To put this rise in weathering intensity in context for soil dynamics, we compare these findings with previous studies on environmental change in the European Alps throughout the Holocene. During the early part of the record (9.5 to 6.2 ky cal BP), physical erosion remained low and relatively stable (Fig. 3), consistent with a warm and dry Early Holocene climate (39, 40). By 9.5 ky cal BP, arboreal vegetation was widespread across the Bourget catchment, though not uniformly distributed (41–46). Similarly, progressive soil development varied with elevation, with well-developed soils in the lowlands and early-stage soils at higher elevations (8, 47–49) (Fig. 4). In addition, the increased smectite input into Lake Bourget during this period (50) is also consistent with the progressive soil formation across the catchment, as reflected in the negative δ^7Li trend between 9.5 and 6.2 ky cal BP (Fig. 3).

A first notable divergence from the decreasing trend in the δ^7Li vs. Li/Al ratio plot occurs between 5.6 and 3.8 ky cal BP (Fig. 2). During this period, the δ^7Li and Li/Al lake sediment signature shifts back toward its initial position within the mixing array, suggesting that a larger proportion of solid material chemically similar to the parent rock, was deposited into the lake. This change is followed by the first significant increase in erosion rate recorded in the catchment (Fig. 3) which has been attributed to cooler and wetter conditions in the European Alps (12, 51) [the "Neo-Glacial" period, (52)]. In the context of increased erosion, we interpret the elevated δ^7Li_{NG}, approaching the signature of the bedrock (Fig. 2), as reflecting significant incision of the land surface, leading to deepening of the hydrographic network and the development of gully-type erosion (Fig. 4). This scenario is supported by the stability of the vegetation cover during this time (45, 46, 53), suggesting that erosion was mainly confined to watercourses, rather than spreading across broader areas, and likely affected the entire catchment uniformly. Overall, the δ^7Li shift at 6.2 ky cal BP (Fig. 4) marks a climate-driven transition from a phase of soil development with limited hillslope erosion under warm, dry conditions (9.5 to 6.2 ky cal BP), to enhanced channel erosion under cooler, wetter conditions (6.2 to 3.8 ky cal BP).

Distinct Influence of Agropastoral Activities on Soil Evolution Across Altitudinal Levels. From 3.8 ky cal BP onward, no clear trend emerges from the δ^7Li vs. Li/Al ratio (Fig. 2). Conversely, the δ^7Li_{NG} record exhibits a recurring pattern of decline followed by a sharp increase across three distinct temporal phases: 3.8 to 3.0 ky cal BP, 2.8 to 1.6 ky cal BP, and 1.6 ky cal BP to modern times. The amplitudes of δ^7Li_{NG} variation in each of these phases are substantial: 0.6, 1.3, and 1.2‰, respectively. The systematic decrease in the δ^7Li_{NG} signal at the onset of all three phases suggests the erosion of more superficial soil horizons, which were not affected by gully-type processes and exhibit isotopic signature most distinct from that of the parent rock (15). The subsequent increase in δ^7Li_{NG} indicates that erosion deepened, reaching lower soil horizons closer in composition to the parent rock. The sequence of these three erosion-driven excursions can be interpreted in two ways: i) widespread increased physical erosion followed by rapid rebuilding or redifferentiation of soil or ii) localized increases in physical erosion limited to one part of the catchment followed by erosion of previously unaffected areas. To discriminate between these two assumptions, we compare the δ^7Li_{NG} variations with proxies of the intensity of agropastoral activities (12, 27)—pollen and environmental DNA data—in eight sediment sequences from lakes located within or near the catchment area. These records highlight the elevation ranges most affected over the past 3,800 y, pinpointing areas where soils likely underwent significant changes (*SI Appendix*, Fig. S6). According to these studies, agropastoral activities have increasingly become

the primary driver of erosion since 3.8 ky cal BP, magnifying climate-related erosion by a factor of two (12). Moreover, the three phases of δ^7Li_{NG} increase correspond to erosive surges associated with the development of successive phases of agropastoral activities occurring at distinct times and elevations (Fig. 3) (12). This suggests that the Li isotope excursions in the Lake Bourget record after 3.8 ky reflect the staggered development of agropastoral activities at different elevations rather than a uniform response throughout the catchment.

In detail, the first erosion surge, occurring between 3.5 and 2.7 ky cal BP, was primarily centered on the high-elevation (2,000 to 3,300 m) portion of the nonglaciated region of the catchment (12). The main driver of this event was the expansion of pastoralism, which led to significant land clearance (12, 27). During this period, the δ^7Li_{NG} signal increases from a yet-unreached very negative value to levels comparable to those observed during the Neoglacial period (Fig. 3). The very low δ^7Li_{NG} value at 3.5 ky cal BP likely reflects the erosion of weathered topsoil horizons (Fig. 2), a scenario supported by the concurrent appearance of organic markers in Lake Bourget sediments (54), interpreted as proxies for the erosion of surficial soil horizons (54, 55). Oxygen and Hydrogen Indices from the high-elevation Lake Anterne (Fig. 1), located in the main locus of erosion during this first surge (27), also indicate an increase in erosion and the transport of organic matter from surface horizons, followed by significant contribution of organic matter from deeper soil horizons (56, 57). The subsequent increase in δ^7Li_{NG} values can be linked to the progressive erosion of deeper soil horizons, closer to the bedrock (Fig. 2). During both the second (2.2 to 1.6 ky cal BP) and third (1.4 to 0.2 ky cal BP) erosive surges, a similar increase in δ^7Li_{NG} is observed (Fig. 3). These trends likely reflect the expansion of agriculture, subsequently intensified by the introduction of the plow and the emergence of more complex agroecosystems, alongside pastoralism at low to mid-elevations (12, 27). While human activity remained pronounced at higher elevations until the end of the second surge (*SI Appendix*, Fig. S6), the increasingly limited soil availability in these areas after the first surge likely limited their contribution to the δ^7Li_{NG} signal in the lake. This interpretation is reinforced by the observed increase of the δ^7Li signal in Lake La Thuile during the second surge, likely reflecting the impact of agricultural activities (16).

Altogether, the first erosive surge primarily affected the upper portion of the nonglaciated catchment area, while the second and third surges were largely confined to lower-elevation areas (below 2,000 m). An interesting observation is the lower initial δ^7Li_{NG} value during the second surge, relative to the first. This indicates that the soil horizons mobilized during this second surge were more weathered than the ones eroded during the first surge at higher elevation (Fig. 4). We suggest that this pattern results from a longer period of pedogenesis in these lower-elevation areas following deglaciation. The subsequent increase in δ^7Li_{NG} values can thus be interpreted as the gradual erosion of progressively deeper soil horizons across different elevation ranges. Notably, the initial δ^7Li_{NG} value of the third surge is less negative than that of the first two, suggesting that soils eroded during this episode had already undergone a prior phase of degradation. Hence, since 3.8 ky cal BP, the δ^7Li_{NG} signal serves as a proxy for the eroded horizon, confirming previous interpretations that erosive surges linked to human activity reflect erosion at specific elevation ranges (below 3,300 m), particularly those where agropastoral activity was concentrated (12).

Implications for Human and Climate Forcing on Soil Evolution. By anchoring our study in the Lake Bourget catchment, where Holocene land-use changes and their impact on soil erosion are particularly well documented, we are able to reconstruct soil development across elevation gradients and delineate pedogenic trajectories shaped by both natural processes and human activity (Fig. 4). These findings underscore the need to account for both spatial and temporal heterogeneity when interpreting δ^7Li records from lake sediments in mountainous settings. This approach, however, is inherently biased toward eroding landscapes, as the δ^7Li signal in detrital sediments reflects areas where physical erosion outpaces soil formation, offering limited insight into stable, noneroding zones. In regions lacking comprehensive paleoenvironmental datasets, future work should aim to systematically combine lithium isotopes with paleoaltitude proxies (e.g., δD of biomarkers, $\delta^{13}C_{org}$) to improve spatial resolution and capture a comprehensive picture of soil evolution in mountainous environments (e.g., refs. 58 and 59).

Our results show that, unlike bioclimatic fluctuations, which tend to drive soil development in a relatively synchronous manner across elevation gradients, agropastoral activities induce a pronounced altitudinal decoupling of pedogenic trajectories, particularly with respect to erosion. Climatic phases such as the Neoglacial or deglaciation periods triggered catchment-wide shifts toward gully erosion and soil development, respectively. After deglaciation, broadly similar sequences of soil development occur across elevations, albeit with time lags due to asynchronous glacial retreat (Fig. 4). These sequences, progressing from Lithosols to Regosols, Cambisols, and eventually Podzols, align with patterns observed elsewhere in the European Alps (8, 47). However, such climate-related lag is later overprinted by the effects of human activity, and importantly, human-driven soil destruction and soil development can occur simultaneously across different elevation ranges (Fig. 4).

Our lithium isotope-based analysis provides quantitative constraints on the relative contributions of soil formation and erosion rates driven by agropastoral activities and climate change. In the initial period of soil formation (9.5 to 3.8 ky cal BP), the climatic change (increase precipitation, decrease temperature) of the Neo-Glacial period, did not hinder soil development despite increase channel erosion. However, the first erosive surge driven by increased agropastoral activities marked the cessation of soil development at high elevations. In mid-elevation areas and foothills, soils thus undergone a longer development period from deglaciation to the second erosive surge. Using the δ^7Li_{NG} signal as a proxy for soil development during this period, we observe an overall decrease in the δ^7Li signature of soils in the catchment by almost 2‰ over 7,300 y (Fig. 3). This corresponds to an average rate of change in soil δ^7Li of approximately 0.3 ‰ per millennium alongside a potential increase in weathering intensity by a factor of about 6 (*SI Appendix*, Fig. S4). Conversely, the short (0.4 to 1 ky) human-triggered erosive surges caused dramatic changes, with soil δ^7Li rates of change ranging from 1.2 to 3.2‰ per ky. As a consequence, climate and human activities have both impacted alpine soils over millennia, but at very different rates. While climate has caused only minimal changes over nearly 10 ky, human activities, primarily agriculture and grazing, have sent alpine soils back to a state resembling that of the Early Holocene within just a few thousand years. While this approach is based on several key assumptions, the difference in rates measured between natural soil formation and soil degradation under the influence of human activities is striking: human activities degrade soils 4 to 10 times faster than they can naturally form. These findings underscore the profound impact of human activities on soils and the Critical Zone.

Building upon this understanding, our results further demonstrate that soil development along elevation gradients is shaped by a dual legacy: natural pedogenic processes tied to glacial retreat

and a superimposed layer of anthropogenic alteration (Fig. 4). The latter signal marks the onset of a pedological Anthropocene (60), in which human activity emerges as the dominant force in soil development. More broadly, it is the functioning of the entire Critical Zone that may be affected. By disentangling the respective contributions of bioclimate evolution and human land use, we provide a clearer understanding of soil trajectories in mountain environments, a pattern likely shared by many mountain regions worldwide. Crucially, this transition does not occur uniformly across the globe. Its timing is closely linked to the spread of Neolithization and the nature of agropastoral systems that followed (9, 61). Our findings place the onset of the pedological Anthropocene around 3.8 ky BP in the European Alps, coinciding with some of the earliest global signals of human-induced soil erosion (9). However, evidence from the Andean Plateau dates it to 2.4 to 1.9 ky BP (62), and in North America, not until the early 19th century (63, 64), highlighting the regional nature of this global transition. These insights highlight the need to integrate both geological and anthropogenic legacies when assessing the functioning and future resilience of soils. Extending such approaches globally is crucial to better understand how agropastoral practices affect soil evolution and guide the development of truly sustainable land-use systems (6, 65).

Materials and Methods

Lake Sediment Sequence and Sample Selection. The sediments of Lake Bourget have been extensively studied (35, 50, 54). Among all the existing sedimentary sequences, we chose to use a 13.7-m long sequence, called "LDB18&19" (IGSN n°TOAE0000000005 & n° TOAE0000000006, 45°44.717′N; 5°51.789′E) collected during two campaigns in June 2018 and June 2019 (12). This sequence covers approximately 9,450 y of record and is located at the lake depocenter. According to age-model uncertainties, all ages are given with a precision of 50 y (12). Fifty-nine 1 cm-thick sediment samples were collected with a constant sampling step of 10 cm for major and trace element concentrations and neodymium (Nd) isotopic composition measurements (11). To characterize the source of sediments accumulated in the Lake Bourget deep basin, 29 river sediment samples were collected between January and February 2018 from flood deposits in the main tributaries and in the Arve and Rhône rivers (12).

Lake and River Sediment Sample Selection. For Li isotope measurements, we selected 27 samples from the lake sediment sequence and 8 from the river sediment samples. The lake sediment samples cover the entire Holocene, whereas the river samples correspond to the main tributaries of the Rhône and Arve rivers and were chosen to characterize the signatures of the two main catchment regions. Each lake sample was processed as bulk sediment. For 5 of them, an aliquot was sieved at 5 μm to obtain the signature of the fine particles entering the lake, as this fraction was identified as one of the two modes of the detrital particle grain size distribution (35). The 8 river sediment samples were sieved at 63 μm, and 5 of them were also sieved at 25 μm to obtain a signature characteristic of fine particles. All samples were first dried at 60 °C for 72 h in a laboratory oven and subsequently crushed in an agate mortar. Powders were then decarbonated by two successive HCl 0.5 N leaching steps to remove authigenic and detrital carbonates. All the samples were then digested in concentrated acid mixtures of HF, HNO_3, and HCl.

Geochemical Analyses. Major and trace element contents were measured using an Agilent 7900 quadrupole ICP-MS at the PARI analytical platform of IPGP. The reported uncertainties were calculated via the algebraic propagation of blank subtraction and sample count SD (n = 3). The NIST®SRM®2709a reference material (San Joaquin soil) was processed as a sample and analyzed repeatedly during the sequences to evaluate the accuracy of the measurements. The detection limit was between 0.2 and 0.5 ppt depending on the element, and the internal errors were 5% on average.

Lithium isotope measurements were performed at the PARI analytical platform of IPGP and at the Arthur Holmes Isotope Geology Laboratory, Dept. of Earth Sciences, Durham University using, at both institutes, a ThermoFisher Neptune Multi-Collector-ICPMS (MC-ICPMS). After HF-HNO_3 digestion of solid samples, Li was separated from the sample matrix by ion-exchange chromatography following the same method as in ref. 33. Elution cuts immediately before and after the Li elution peak were collected for each sample and checked for the absence of Li. The eluates with a loss equal to or greater than 0.5% of the total mass of Li loaded were discarded, to avoid any significant effect of isotope fractionation occurring during Li elution. Repeated measurements of the seawater NASS-6 reference material yielded δ^7Li = +31.42 ± 0.40 ‰ (±2σ, n = 6 separations) whereas repeated measurements of the soil NIST®SRM®2709a reference material yielded δ^7Li = −0.30 ± 0.51 ‰ (±2σ, n = 6 separations, 4 digestions), and those of the basalt JB2 reference material yielded δ^7Li = +5.36 ± 0.58 ‰ (±2σ, n = 5 separations, 4 digestions). In this study, we use the uncertainty obtained on NASS-6 (±0.40 ‰), the reference material measured the most during our sessions. The concentration of the total procedural blank (acid digestion and column chemistry) was assessed to be less than 0.05 ng, which is negligible compared with the amount of Li loaded onto the column (i.e., 25 to 200 ng).

Uncertainties on the δ^7Li_{NG} Signal. A Monte Carlo method was used to compute uncertainties in the fractional contributions based on Nd isotopes (12). Random sampling within the analytical uncertainties of each parameter was executed via a Box–Muller transform (66) for each of the 5,000 iterations of the Monte Carlo procedure on Excel software.

Lithium Mixing Model. A mixing model was established to describe the relationship between the two main sediment sources in the catchment in a δ^7Li and Li/Al biplot (Fig. 2). The river sediment sample taken from the foot of the Mont-Blanc massif was selected as the glaciated (granite) endmember, whereas the bedrock from the Lake La Thuile catchment was selected as the nonglaciated (sedimentary cover) endmember. A Monte Carlo method similar to the one used for the δ^7Li_{NG} signal was used to compute uncertainties in the fractional contributions to the Li budget of the lake sediment.

$$f_G + f_{NG} = 1, \quad [4]$$

$$Li/Al_{Mix} = Li/Al_G \times f_G + Li/Al_G \times f_{NG}, \quad [5]$$

$$\delta^7Li_{Mix} = \frac{\delta^7Li_G \times Li/AL_G \times f_G}{Li/AL_{Mix}} + \frac{\delta^7Li_{NG} \times Li/AL_{NG} \times f_{NG}}{Li/AL_{Mix}}. \quad [6]$$

Data, Materials, and Software Availability. All data are included in the manuscript and/or *SI Appendix*.

ACKNOWLEDGMENTS. This work was cofinanced by the "CRITLAKE" project, cofunded by the Ecosphère Continentale et Côtière (EC2CO) CNRS program and appel à projets (AAP) Université Savoie Mont-Blanc. Parts of this work were also supported by the Institut de Physique du Globe de Paris multidisciplinary program Plateforme d'analyse haute résolution (PARI) and by Paris-Ile de France region "SESAME" Grant No. 12015903. This project also received funding from the European Research Council (ERC) under the European Union's Horizon Europe Research and Innovation Program (ERC Starting Grant LAKE-SWITCH, No. 101041998 to M.D.). We are grateful to Pierre Burckel for help with major and traces measurements; to Laëticia Faure for her valuable help and assistance with lab work; to Akanksha Praharaj for assisting with Li isotopes chemistry and lithium isotopes measurements; to Pascale Louvat, Thibaud Sondag, Barthélémy Julien, and Dimitri Rigoussen for assistance with lithium isotopes measurements at Institut de Physique du Globe de Paris; to Julia Garagnon for the help with the synthesis figure; and to Geoff Nowel for valuable help and assistance with laboratory work and lithium isotopes measurements at the Earth Science Department of Durham University.

Author affiliations: [a]Laboratoire Environnements, Dynamiques et Territoires de Montagne (EDYTEM), CNRS, Université Savoie Mont-Blanc, Chambéry 73000, France; [b]Department of Earth Sciences, Durham University, Durham DH1 3LE, United Kingdom; [c]Institut de Physique Du Globe de Paris, Université Paris Cité, CNRS, Paris 75005, France; and [d]Laboratoire Géosciences Paris-Saclay (GEOPS), Université Paris Saclay, Orsay 91405, France

1. D. D. Richter *et al.*, Earth sciences are the model sciences of the Anthropocene. *Perspect. Earth Space Sci.* **5**, e2024CN000237 (2024), 10.1029/2024CN000237.
2. FAO, *Status of the World's Soil Resources (SWSR)–Main Report* (Food and Agriculture Organization, UN Intergovernmental Technical Panel on Soils, Rome, Italy, 2015), vol. **650**.
3. P. R. Shukla *et al.*, "Technical summary" in *Climate Change and Land: An IPCC Special Report on Climate Change, Desertification, Land Degradation* (Food Security, and Greenhouse Gas Fluxes in Terrestrial Ecosystems, Sustainable Land Management, 2019).
4. L. Montanarella, Agricultural policy: Govern our soils. *Nature* **528**, 32–33 (2015).
5. P. Borrelli *et al.*, An assessment of the global impact of 21st century land use change on soil erosion. *Nat. Commun.* **8**, 2013 (2017).
6. D. R. Montgomery, Soil erosion and agricultural sustainability. *Proc. Natl. Acad. Sci. U.S.A.* **104**, 13268–13272 (2007).
7. P. Borrelli *et al.*, Land use and climate change impacts on global soil erosion by water (2015–2070). *Proc. Natl. Acad. Sci. U.S.A.* **117**, 21994–22001 (2020).
8. M. Bajard *et al.*, Long-term changes in alpine pedogenetic processes: Effect of millennial agro-pastoralism activities (French–Italian Alps). *Geoderma* **306**, 217–236 (2017).
9. J.-P. Jenny *et al.*, Human and climate global-scale imprint on sediment transfer during the holocene. *Proc. Natl. Acad. Sci. U.S.A.* **116**, 22972–22976 (2019).
10. H. Zhao *et al.*, Quantifying the dynamic processes of soil erosion and lake sediment deposition in the Holocene in China. *Q. Sci. Rev.*, **304**, 107993 (2023).
11. W. Rapuc *et al.*, Quantitative evaluation of human and climate forcing on erosion in the alpine Critical Zone over the last 2000 years. *Q. Sci. Rev.* **268**, 107127 (2021), 10.1016/j.quascirev.2021.107127.
12. W. Rapuc *et al.*, Human-triggered magnification of erosion rates in European Alps since the Bronze Age. *Nat. Commun.* **15**, 1246 (2024).
13. F. Arnaud *et al.*, Erosion under climate and human pressures: An alpine lake sediment perspective. *Q. Sci. Rev.* **152**, 1–18 (2016). 10.1016/j.quascirev.2016.09.018152.
14. K. Mills *et al.*, Deciphering long-term records of natural variability and human impact as recorded in lake sediments: A palaeolimnological puzzle. *WIREs Water* **4**, e1195 (2017), 10.1002/wat2.1195.
15. L. Rothacker *et al.*, Impact of climate change and human activity on soil landscapes over the past 12, 300 years. *Sci. Rep.* **8**, 247 (2018).
16. X. Zhang *et al.*, Evolution of the alpine critical zone since the Last Glacial Period using Li isotopes from lake sediments. *Earth Planet. Sci. Lett.* **624**, 118463 (2023).
17. L. Bastian *et al.*, Co-variations of climate and silicate weathering in the Nile basin during the late Pleistocene. *Q. Sci. Rev.* **264**, 107012 (2021), 10.1016/j.quascirev.2021.107012.
18. K. W. Burton, N. Vigier, "Lithium isotopes as tracers in marine and terrestrial environments" in *Handbook of Environmental Isotope Geochemistry*, M. Baskaran, Ed. (Springer, 2012), vol. **I**, pp. 41–59.
19. Y. Huh, L.-H. Chan, L. Zhang, J. M. Edmond, Lithium and its isotopes in major world rivers: Implications for weathering and the oceanic budget. *Geochim. Cosmochim. Acta* **62**, 2039–2051 (1998).
20. J. S. Pistiner, G. M. Henderson, Lithium-isotope fractionation during continental weathering processes. *Earth Planet. Sci. Lett.* **214**, 327–339 (2003).
21. P. A. E. Pogge von Strandmann *et al.*, The lithium isotope response to the variable weathering of soils in Iceland. *Geochim. Cosmochim. Acta* **313**, 55–73 (2021).
22. E. Lemarchand, F. Chabaux, N. Vigier, R. Millot, M.-C. Pierret, Lithium isotope systematics in a forested granitic catchment (Strengbach, Vosges Mountains, France). *Geochim. Cosmochim. Acta* **74**, 4612–4628 (2010).
23. Y. Huh, L. Chan, O. A. Chadwick, Behavior of lithium and its isotopes during weathering of Hawaiian basalt. *Geochem. Geophys. Geosyst.* **5**, 2004GC000729 (2004).
24. R. L. Rudnick, P. B. Tomascak, H. B. Njo, L. R. Gardner, Extreme lithium isotopic fractionation during continental weathering revealed in saprolites from South Carolina. *Chem. Geol.* **212**, 45–57 (2004).
25. J.-W. Zhang *et al.*, Lithium and its isotopes behavior during incipient weathering of granite in the eastern Tibetan Plateau, China. *Chem. Geol.* **559**, 119969 (2021).
26. J. K. Golla *et al.*, The evolution of lithium isotope signatures in fluids draining actively weathering hillslopes. *Earth Planet. Sci. Lett.* **567**, 116988 (2021), 10.1016/j.epsl.2021.116988.
27. C. Giguet-Covex *et al.*, Long-term trajectories of mountain agro-ecosystems in the North-Western Alps. *Reg. Environ. Change* **23**, 58 (2023).
28. U. Büntgen *et al.*, 2500 years of European climate variability and human susceptibility. *Science* **331**, 578–582 (2011).
29. J.-P. Jenny *et al.*, A 4D sedimentological approach to reconstructing the flood frequency and intensity of the Rhône River (Lake Bourget, NW European Alps). *J. Paleolimnol.* **51**, 469–483 (2014).
30. M. Revel-Rolland *et al.*, Sr and Nd isotopes as tracers of clastic sources in Lake Le Bourget sediment (NW Alps, France) during the Little Ice Age: Palaeohydrology implications. *Chem. Geol.* **224**, 183–200 (2005).
31. P. Panagos *et al.*, Estimating the soil erosion cover-management factor at the European scale. *Land Use Policy* **48**, 38–50 (2015).
32. M. Rossi, *Déformation, Transferts de Matière et de Fluide dans La CroÛte Continentale: Application aux Massifs Cristallins Externes des Alpes* (Université Joseph Fourier (Grenoble 1971–2015), 2005).
33. M. Dellinger *et al.*, Lithium isotopes in large rivers reveal the cannibalistic nature of modern continental weathering and erosion. *Earth Planet. Sci. Lett.* **401**, 359–372 (2014).
34. M. Dellinger, J. Bouchez, J. Gaillardet, L. Faure, J. Moureau, Tracing weathering regimes using the lithium isotope composition of detrital sediments. *Geology* **45**, 411–414 (2017).
35. F. Arnaud, Discriminating bio-induced and detrital sedimentary processes from particle size distribution of carbonates and non-carbonates in hard water lake sediments. *J. Paleolimnol.* **34**, 519–526 (2005).
36. M. Gardent, A. Rabatel, J.-P. Dedieu, P. Deline, Multitemporal glacier inventory of the French Alps from the late 1960s to the late 2000s. *Glob. Planet. Change* **120**, 24–37 (2014).
37. C. Yang, N. Vigier, S. Yang, M. Revel, L. Bi, Clay Li and Nd isotopes response to hydroclimate changes in the Changjiang (Yangtze) basin over the past 14, 000 years. *Earth Planet. Sci. Lett.* **561**, 116793 (2021).
38. J. Seguinot *et al.*, Modelling last glacial cycle ice dynamics in the Alps. *Cryosphere* **12**, 3265–3285 (2018).
39. O. Heiri, B. Ilyashuk, L. Millet, S. Samartin, A. F. Lotter, Stacking of discontinuous regional palaeoclimate records: Chironomid-based summer temperatures from the Alpine region. *Holocene* **25**, 137–149 (2015).
40. S. A. Marcott, J. D. Shakun, P. U. Clark, A. C. Mix, A reconstruction of regional and global temperature for the past 11, 300 years. *Science* **339**, 1198–1201 (2013).
41. J.-L. de Beaulieu *et al.*, Dynamique forestière holocène dans la haute vallée de l'Arve (Haute-Savoie) et migrations de Abies et Picea dans les Alpes occidentales. Festschrift Zoller. *Diss. Bot.* 196, 387–398 (1992).
42. A. A. Ali *et al.*, The early holocene treeline in the Southern French Alps: New evidence from travertine formations. *Glob. Ecol. Biogeogr.* **12**, 411–419 (2003).
43. F. David, An example of the consequences of human activities on the evolution of subalpine landscapes. *C. R. Palevol.* **9**, 229–235 (2010).
44. J. Argant, C. Bégeot, Y. Marrocchi, *L'environnement Végétal au Tardiglaciaire à Partir de L'étude Pollinique de Trois Lacs* (Société Préhistorique Française, 2008), p. 23.
45. E. Doyen *et al.*, Land use development and environmental responses since the Neolithic around Lake Paladru in the French Pre-alps. *J. Archaeol. Sci. Rep.* **7**, 48–59 (2016).
46. M. Bajard *et al.*, Erosion record in Lake La Thuile sediments (Prealps, France): Evidence of montane landscape dynamics throughout the Holocene. *Holocene* **26**, 350–364 (2016).
47. B. Mourier, J. Poulenard, C. Carcaillet, D. Williamson, Soil evolution and subalpine ecosystem changes in the French Alps inferred from geochemical analysis of lacustrine sediments. *J. Paleolimnol.* **44**, 571–587 (2010).
48. M. Egli, A. Mirabella, P. Fitze, Formation rates of smectites derived from two Holocene chronosequences in the Swiss Alps. *Geoderma* **117**, 81–98 (2003).
49. E. Brisset *et al.*, Lateglacial/Holocene environmental changes in the Mediterranean Alps inferred from lacustrine sediments. *Q. Sci. Rev.* **110**, 49–71 (2015).
50. M. Debret *et al.*, North western Alps Holocene paleohydrology recorded by flooding activity in Lake Le Bourget. *Q. Sci. Rev.* **29**, 2185–2200 (2010).
51. N. P. McKay *et al.*, The 4.2 ka event is not remarkable in the context of holocene climate variability. *Nat. Commun.* **15**, 6555 (2024).
52. P. Deline, G. Orombelli, Glacier fluctuations in the western Alps during the Neoglacial, as indicated by the Miage morainic amphitheatre (Mont Blanc Massif, Italy). *Boreas* **34**, 456–467 (2005).
53. C. Heiri, H. Bugmann, W. Tinner, O. Heiri, H. Lischke, A model-based reconstruction of Holocene treeline dynamics in the central Swiss Alps. *J. Ecol.* **94**, 206–216 (2006).
54. J. Jacob *et al.*, Impacts of new agricultural practices on soil erosion during the Bronze Age in the French Prealps. *Holocene* **19**, 241–249 (2009).
55. S. G. Wakeham, E. A. Canuel, Biogenic polycyclic aromatic hydrocarbons in sediments of the San Joaquin River in California (USA), and current paradigms on their formation. *Environ. Sci. Pollut. Res.* **23**, 10426–10442 (2016).
56. J. Pansu *et al.*, Reconstructing long-term human impacts on plant communities: An ecological approach based on lake sediment DNA. *Mol. Ecol.* **24**, 1485–1498 (2015).
57. C. Giguet-Covex *et al.*, Changes in erosion patterns during the Holocene in a currently treeless subalpine catchment inferred from lake sediment geochemistry (Lake Anterne, 2063 m.a.s.l., NW French Alps): The role of climate and human activities. *Holocene* **21**, 651–665 (2011).
58. J. Wang *et al.*, Long-term patterns of hillslope erosion by earthquake-induced landslides shape mountain landscapes. *Sci. Adv.* **6**, eaaz6446 (2020).
59. C. Ponton, A. J. West, S. J. Feakins, V. Galy, Leaf wax biomarkers in transit record river catchment composition. *Geophys. Res. Lett.* **41**, 6420–6427 (2014).
60. G. Certini, R. Scalenghe, Anthropogenic soils are the golden spikes for the Anthropocene. *Holocene* **21**, 1269–1274 (2011).
61. N. Dubois *et al.*, First human impacts and responses of aquatic systems: A review of palaeolimnological records from around the world. *Anthropol. Rev.* **5**, 28–68 (2018).
62. K. Hippe *et al.*, Cosmogenic in situ ^{14}C–^{10}Be reveals abrupt late Holocene soil loss in the Andean Altiplano. *Nat. Commun.* **12**, 2546 (2021).
63. S. B. Penprase *et al.*, Plow versus Ice Age: Erosion rate variability from glacial—interglacial climate change is an order of magnitude lower than agricultural erosion in the Upper Mississippi River Valley, USA. *Geology* **153**, 535–539 (2025), 10.1130/G52585.
64. D. B. Kemp, P. M. Sadler, V. Vanacker, The human impact on North American erosion, sediment transfer, and storage in a geologic context. *Nat. Commun.* **11**, 6012 (2020).
65. D. D. Richter, Game changer in soil science. The Anthropocene in soil science and pedology. *J. Plant Nutr. Soil Sci.* **183**, 5–11 (2020).
66. G. E. P. Box, M. E. Muller, A note on the generation of random normal deviates. *Ann. Math. Stat.* **29**, 610–611 (1958).